Electronic Supplementary Material (ESI) for Journal of Materials Chemistry A.

Supporting information

Using nanoconfinement to inhibit the degradation pathways of conversion-metal oxide anodes for highly stable fast-charging Li-ion batteries

Benjamin Ng, Xiong Peng, Ehsan Faegh, and William E. Mustain*

Department of Chemical Engineering, Swearingen Engineering Center, University of South Carolina, Columbia, SC 29208, United States

*Corresponding author: Email: mustainw@mailbox.sc.edu; Phone: 803-576-6393

Transmission Electron Microscopy (TEM): Pre/Post-cycled

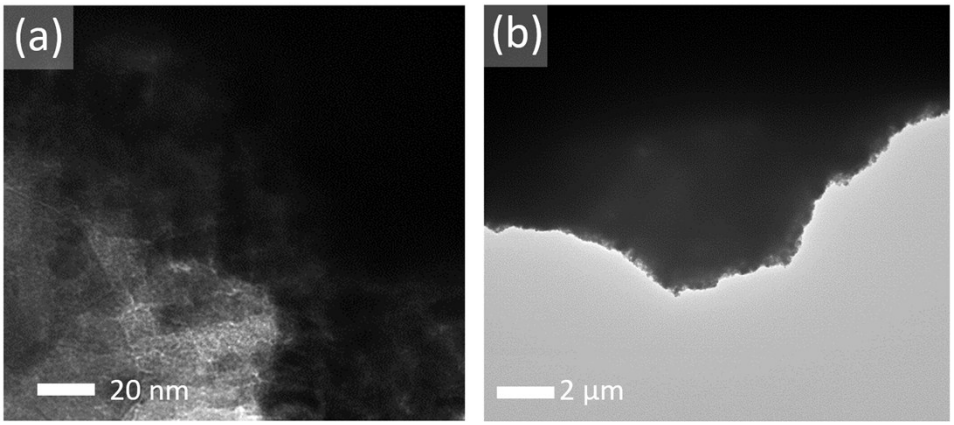

Figure S1. Post-cycled images of NiO/C after 100 cycles

In order to lay the basis for the modified 3-electrode TEM experiment reported in the main document, 10x and 100x post-cycled experiments were conducted. After 100 cycles, the material completely lost all boundaries that were attributed to the order-mesoporous NiO originally synthesized. Subsequently, all additional post-cycled TEM characterization was done at 10 cycles for consistent comparison.

Material Characterization and analysis:

X-Ray Diffraction (XRD) Analysis was used to determine the crystallite domain size by applying the Scherrer equation below:

$$L_{CDS} = \frac{K\lambda}{\beta cos\theta}$$

where the X-ray wavelength (λ) is in nm, the full width half maximum (FWHM) is β, the shape factor is K.

Table S1. Crystallite domain size at NiO (111) peak in the XRD pattern

	Peak Position (2Theta)	**Full Width Half Maximum (2Theta)**	**Crystallite Domain Size (nm) Sherrer Eqn**
NiO/C	37.4	0.34	25.77
ID-NiO@CNT	37.36	0.64	13.69
NC-NiO@CNT	37.34	0.6	14.6

Table S2. Crystallite domain size at NiO (200) peak in the XRD pattern

	Peak Position (2Theta)	Full Width Half Maximum (2Theta)	Crystallite Domain Size (nm) Sherrer Eqn
NiO/C	43.46	0.36	24.82
ID-NiO@CNT	43.28	0.46	19.41
NC-NiO@CNT	43.3	0.52	17.18

Table S3. Crystallite domain size at NiO (220) peak in the XRD pattern

	Peak Position (2Theta)	Full Width Half Maximum (2Theta)	Crystallite Domain Size (nm) Sherrer Eqn
NiO/C	63.00	0.44	22.13
ID-NiO@CNT	62.82	0.48	20.26
NC-NiO@CNT	62.78	0.44	22.10

Table S4. Crystallite domain size at NiO (222) peak in the XRD pattern

	Peak Position (2Theta)	Full Width Half Maximum (2Theta)	Crystallite Domain Size (nm) Sherrer Eqn
NiO/C	75.52	0.50	21.00
ID-NiO@CNT	75.34	0.50	20.98
NC-NiO@CNT	75.36	0.52	20.17

Electrochemical performance of Nanoconfined NiO:

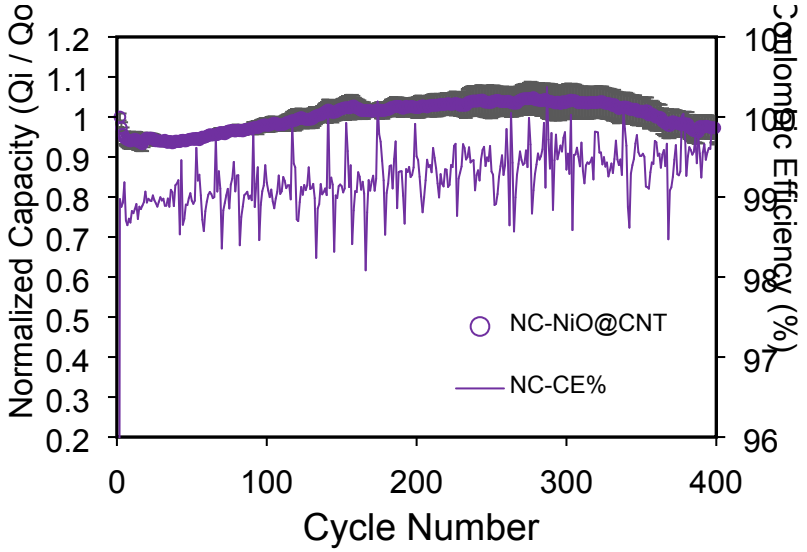

Figure S2. Extended normalized capacity retention (Q_i/Q_o) from Figure 1 in the main document

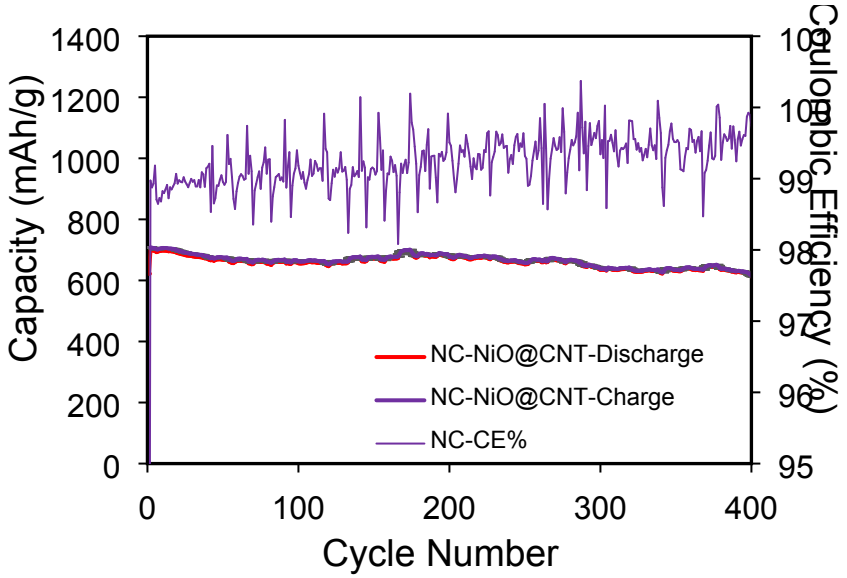

Figure S3. Gravimetric capacity of NC-NiO@CNT_{50}

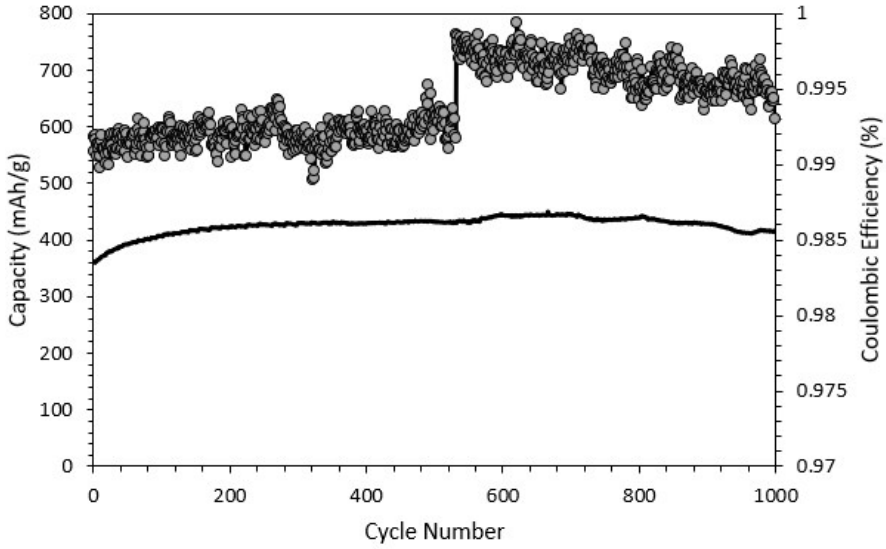

Figure S4. High rate (5C) capacity retention for NC-NiO@CNT_{50}. Note, the jump in coulombic efficiency is due to shutdown of the Arbin MSTAT Battery cycler from a power outage.

Stepwise degradation pathways in Non-confined MO

Though Equation 1 gave the over-arching chemistry for the conversion of MO (e.g. NiO) anodes in Li-ion batteries, that reaction is not able to capture a necessary level of detail that can describe the degradation pathways. Thus, near-elementary steps that occur during the NiO conversion reaction are provided in Equations 3-8[1–3] in Table 1. During the charge (reduction), Li desolvation occurs at the SEI/bulk electrolyte interface and then undergoes inclusion into the SEI

- which in the previously discussed degradation pathway for NiO/C and ID-NiO/CNT, the uncontrolled growth of the SEI can lead to decreased ionic conductivity (i.e. loss of electrolyte due to irreversible reduction) and high diffusion barrier (i.e. denser and thicker SEI). The propagation of Li^+_{SEI} through the SEI migrates to the bulk NiO (≡NiO-NiO) interface to form a $\equiv \mathrm{NiO} - NiO\text{ - }Li$ junction. Next, oxygen displacement occurs to form an $\equiv NiO - Ni^+_{ads}LiO^-_{ads}$. Thermodynamically, Li_2O exists at a lower energy state which makes the chemical reaction of Li^+_{SEI} and $\equiv NiO - Ni^+_{ads}LiO^-_{ads}$ highly favorable and represented in Equation 7. During the nucleation event, the oxygen vacant $\equiv NiO - Ni^+_{ads}$ reduces to $\equiv NiO -$ Ni. Based on the minimization of surface free energy ($^{\sigma_{Ni} > \sigma_{Li_2O}}$), any Ni that exists on the surface of the nucleation platform will exhibit a driving force for spontaneous rearrangement, and Li_2O or other low surface free energy materials will phase segregate to the surface.

In addition, during charge/discharge cycles electrochemical Ostwald ripening will result in the formation of ever-larger crystals, which leads to continual growth of particles and decrease in charge carriers at electrochemically active sites. The Ni-core of large crystals can therefore become electrically and ionically isolated (via a large Li_2O and NiO shell) and lead to trapped Ni metal within the bulk material. Furthermore, the destabilized oxygen balance due to the spontaneous phase segregation of Li_2O, leads to higher interface oxygen content than that within the Ni agglomerates, and therefore promotes the evolution to higher oxidation states ($Ni^{2+} \rightarrow Ni^{3+}$) during the discharge (oxidation) event as seen in NiO/C and ID-NiO/CNT. When the electron flow switches during charge (reduction), the unstable higher oxidation states (Ni^{3+}) follow the proposed irreversible reaction outlined in Equation 2 of the main document. The continuous oxygen-loss due to the uncontrolled formation of the SEI leads to the hypothesis that majority of the degradation pathways in NiO/C and ID-NiO/CNT are a product of architecture and can be controlled by full MO confinement as discussed in the next section.

Table S3. Reaction description and mechanism for the transport of Li^+ from the bulk electrolyte to conversion of NiO to Ni

Equation	Description	Reaction Mechanism
(1)	Li desolvation at the SEI/bulk electrolyte interface	$Li^+_{solvated} \rightleftharpoons Li^+$
(2)	Li transport through the SEI	$Li^+ + \equiv SEI \rightleftharpoons Li^+_{SEI}$
(3)	Junction Formation	$Li^+_{SEI} + \equiv \mathrm{NiO} - NiO + e^- \rightleftharpoons \equiv \mathrm{NiO} - NiO\text{ - }Li$
(4)	Displacement	$\equiv \mathrm{NiO} - NiO\text{ - }Li \rightleftharpoons \equiv NiO - Ni^+_{ads}LiO^-_{ads}$
(5)	Li_2O Formation	$\equiv NiO - Ni^+_{ads}LiO^-_{ads} + Li^+_{SEI} \rightleftharpoons \equiv NiO - Ni^+_{ads} + Li_2O$
(6)	Ni nucleation	$\equiv NiO - Ni^+_{ads} + e^- \rightleftharpoons \equiv NiO - \mathrm{Ni}$

≡ Denotes bulk material

Physical and electrochemical characterization

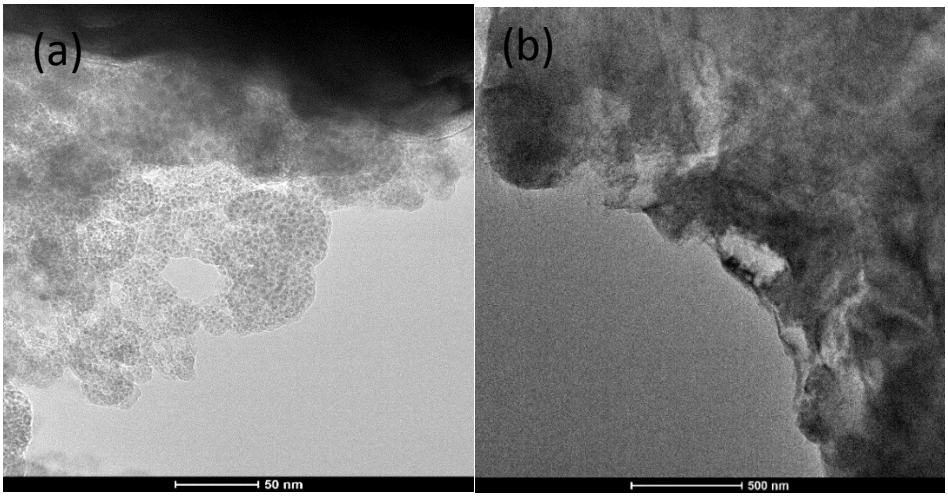

Figure S5. (a)SEI-cluster formation on NiO/C due to repetitive phase separation/recombination during charge/discharge. The aggregative growth of the SEI spans for greater that 50nm.(b) Aggregative growth for greater than 500 nm of NiO/C and complete collapse of the nanostructure.

Scanning Electron Microscopy (SEM): Pre-cycled

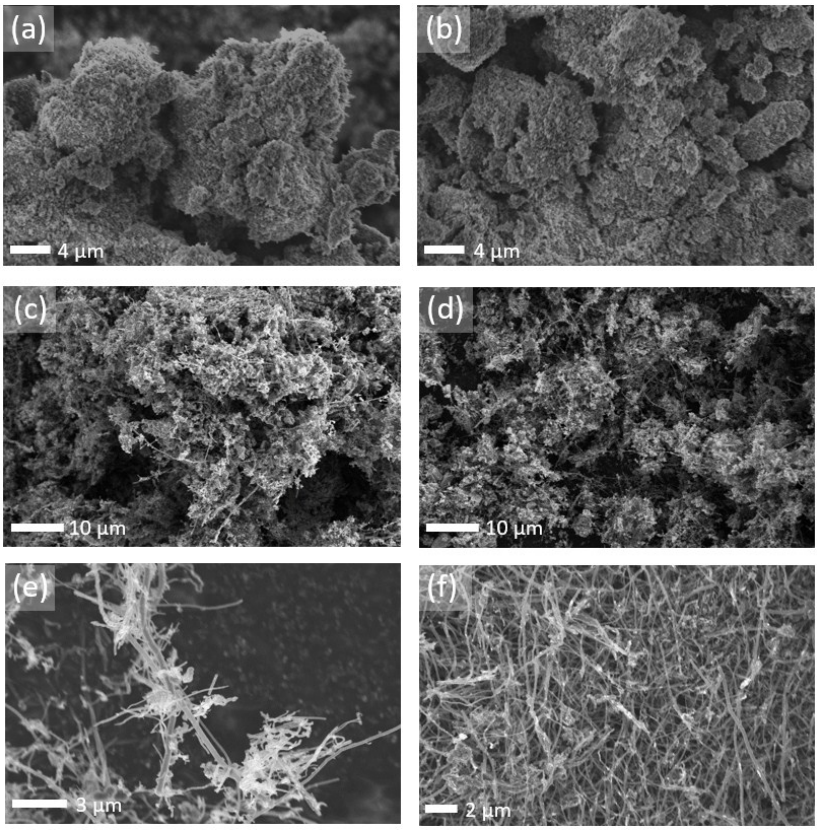

Figure S6. SEM of (a,b) NiO/C, (c,d) ID-NiO/CNT, (e,f) NC-NiO@CNT

Thermogravimetric analysis (TGA):

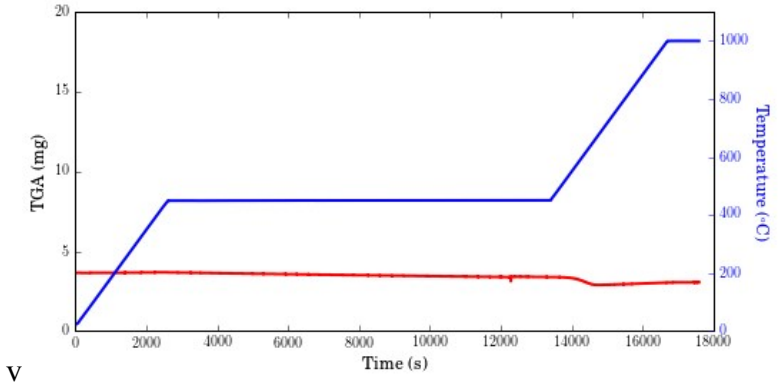

v

Figure S7. Thermo-gravimetric analysis of NC-NiO@CNT_{10}. The plot shows a temperature ramp up from room temperature (~20°C) to 1000°C with a temperature hold at 450°C to remove moisture. The total mass loss of approximately 10.1% (initial mass: 3.317, final mass: 3.688). The total NiO content was determined to be 89.9% active material.

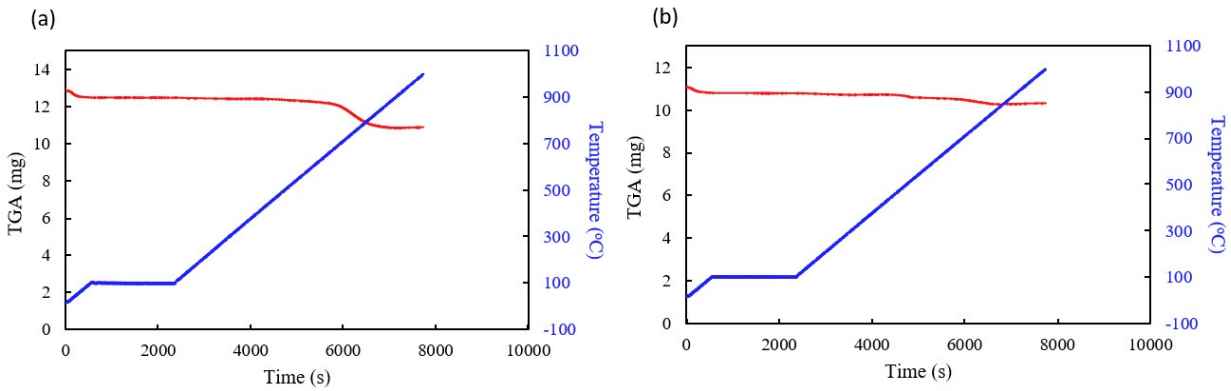

Figure S8. Thermo-gravimetric analysis of (a) ID-NiO/CNT and (b) NC-NiO@CNT_{50}. The plot shows a temperature ramp up from room temperature (~20°C) to 1000°C with a temperature hold at 100°C to remove moisture. The total mass loss of ID-NiO/CNT was approximately 4.1% (initial mass: 10.70, final mass: 10.26). The total NiO content for ID-NiO/CNT was determined to be 95.9% active material. The total mass loss of NC-NiO@CNT_{50} was approximately 12.6% (initial mass: 12.41, final mass: 10.85). The total NiO content for NC-NiO/CNT was determined to be 87.4% active material.

Pre/Post-cycled X-ray Diffraction of NC-NiO@CNT$_{10}$: Reversibility

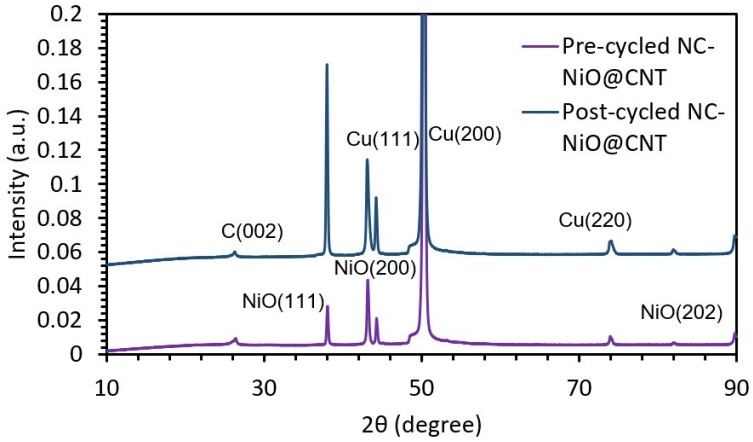

Figure S9. Depicts the XRD patterns for NC-NiO@CNT$_{10}$ pre-cycled and post-cycled electrodes after 1 cycle, and indicates

References

1. Palmieri, A., Spinner, N., Zhao, S. & Mustain, W. E., "Explaining the role and mechanism of carbon matrices in enhancing reaction reversibility of metal oxide anodes for high performance Li ion batteries". *Carbon*, **130** (2018) 515–524.
2. Jow, T. R., Delp, S. A., Allen, J. L., Jones, J.-P. & Smart, M. C., "Factors Limiting Li^+ Charge Transfer Kinetics in Li-Ion Batteries", *J. Electrochem. Soc.*, **165** (2018) A361–A367.
3. Soto, F. A., Marzouk, A., El-Mellouhi, F. & Balbuena, P. B., "Understanding Ionic Diffusion through SEI Components for Lithium-Ion and Sodium-Ion Batteries: Insights from First-Principles Calculations", *Chem. Mater.*, **30** (2018) 3315–3322.